Nuclear Engineering and Technology 53 (2021) 2371–2376

Contents lists available at ScienceDirect

Nuclear Engineering and Technology

journal homepage: www.elsevier.com/locate/net

Original Article

High performance γ-ray imager using dual anti-mask method for the investigation of high-energy nuclear materials

Taewoong Lee [a], Wonho Lee [b, c, *]

[a] Global Institute of Technology, KEPCO KPS, 211, Munhwa-ro, Naju, Jeollanam-do, 58326, Republic of Korea
[b] School of Health and Environmental Science, 145, Anam-ro, Seongbuk-gu, Seoul, 02841, Republic of Korea
[c] BK21 FOUR R&E Center for Learning Health Systems, 145, Anam-ro, Seongbuk-gu, Seoul, 02841, Republic of Korea

ARTICLE INFO

Article history:
Received 2 July 2020
Received in revised form
2 January 2021
Accepted 25 January 2021
Available online 1 February 2021

Keywords:
Dual anti-mask method
Hybrid update maximum likelihood expectation maximization (h-MLEM)

ABSTRACT

As the γ-ray energy increases, a reconstructed image becomes noisy and blurred due to the penetration of the γ-ray through the coded mask. Therefore, the thickness of the coded mask was increased for high energy regions, resulting in severely decreased the performance of the detection efficiency due to self-collimation by the mask. In order to overcome the limitation, a modified uniformly redundant array γ-ray imaging system using dual anti-mask method was developed, and its performance was compared and evaluated in high-energy radiation region. In the dual anti-mask method, the two shadow images, including the subtraction of background events, can simultaneously contribute to the reconstructed image. Moreover, the reconstructed images using each shadow image were integrated using a hybrid update maximum likelihood expectation maximization (h-MLEM). Using the quantitative evaluation method, the performance of the dual anti-mask method was compared with the previously developed collimation methods. As the shadow image which was subtracted the background events leads to a higher-quality reconstructed image, the reconstructed image of the dual anti-mask method showed high performance among the three collimation methods. Finally, the quantitative evaluation method proves that the performance of the dual anti-mask method was better than that of the previously reconstruction methods.

1. Introduction

A coded aperture imaging, which provides a high efficiency high resolution in the reconstructed image of the γ-ray, is used to monitor the nuclear materials emitting γ-rays [1–5]. Among the various types of coded apertures, the squared-shaped modified uniformly redundant array (MURA), which is suitable with common photo devices, has been utilized for the nuclear medicine, astrophysics, industrial applications, decontamination and decommissioning (D&D) [6–10]. The concept of the MURA coded mask was proposed by Gottesman and Fenimore and showed the performance of high sensitivity and high signal to noise ratio (SNR) [6]. To improve the detection efficiency and the field of view (FOV), Smith et al. (2011) built a hybrid portable gamma camera using MURA coded mask [11]. Moreover, the performance of the Compton images was improved due to the angular uncertainty was diminished by mask. In 2017, the portable panoramic γ-ray imaging systems using MURA coded mask were developed, and the reconstructed images which was extended FOV demonstrated the accurate localization of the radioactive sources [12]. Because of the penetration of the radiation through the mask as increasing radiation energies, the performance of the reconstructed image which was blurred decreased. Hence a thick collimator is required for high energy γ-ray imaging however the detection efficiency of the reconstructed γ-ray imaging was decreased due to self-collimation by the mask. Therefore, to improve the image performance of mechanical collimation method, it is crucial to reduce the background events such as scattered radiation or penetration of radiation in the mask. To improve the performance of the radiation detection in rapidly changing background events, Kim et al. (2016) proposed rotating modulation collimator (RMC) with Cs_2LiYCl_6:Ce (CLYC) scintillation detector for dual-particles (neutron and γ-ray) detection and imaging [13]. The characterization and performance of CLYC detector for reconstructed images of dual-particles were evaluated by using MCNP6 codes [14]. The MURA coded mask is

* Corresponding author. School of Health and Environmental Science, 145, Anam-ro, Seongbuk-gu, Seoul, 02841, Republic of Korea.
E-mail address: wonhol@korea.ac.kr (W. Lee).

https://doi.org/10.1016/j.net.2021.01.027

anti-symmetric upon 90° rotation; therefore, it was used for the subtraction of background noise, which is known as the "anti-mask method." The anti-mask subtraction method was used as X-ray and γ-ray imaging since it has advantage of the improved performance of the reconstructed image [15].

As the shadow of the mask pixels using the background subtraction methods provides the results of a high-performance, the reconstructed image using the anti-mask method has been demonstrated to have better performance than that using the conventional only-mask method [15–17]. In the anti-mask method, the two different shadow images can be generated for source reconstruction. The first shadow image can be obtained by subtracting the recorded shadow image of the anti-mask from the recorded shadow image of the only-mask. Subsequently, the second shadow image can be obtained in reverse order. Even though the second shadow image was useful information, it was not used for the reconstruction image. Generally, only the first shadow image is used for source reconstruction. However, the performance of the reconstructed image will be improved if the two different shadow images using the background subtraction method can be utilized to reconstruct the image.

In this study, a compact MURA coded mask imaging system using dual-anti mask method was developed, and its performance was compared and evaluated for high energy radiation sources. In the dual anti-mask method, the information of not only the first shadow image but also the second shadow image was simultaneously used to reconstruct the radiation images of all γ-ray energies. Subsequently, to integrate data from the two different shadow images, the hybrid update maximum likelihood expectation maximization (h-MLEM) method was applied. The performance of the dual-anti mask method is described and compared with previously developed conventional collimation methods. The results of this study demonstrated that the background noise of the dual-anti mask was significantly lower and its performance was higher than the conventional method.

2. Material and methods

As shown in Figs. 1 and 2, a compact MURA coded mask imaging system, Cesium iodide (CsI) scintillator coupled to a position-sensitive photomultiplier tube (PSPMT) [18,19], read-out circuit, field-programmable gate array (FPGA, SPARTAN 3 E), and data-acquisition (DAQ) board (NI 9178). The MURA coded mask that comprised of tungsten was 73 mm × 73 mm × 5 mm in size, while each pixel was 2 mm × 2 mm × 5 mm. The CsI scintillator detector consisted of 20 × 20 pixels with a size 2 mm × 2 mm × 5 mm each.

Fig. 3 shows a schematic diagram of a compact γ-ray imaging system and each modality of collimation methods. The signals from the detector were amplified in the front-end circuit, and the amplitude information was collected using the DAQ board. The

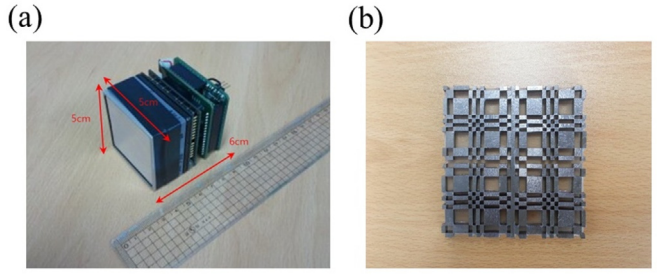

Fig. 1. (a) A compact γ-ray imaging system and (b) MURA coded aperture with a basic 11 × 11 and enlarge to double.

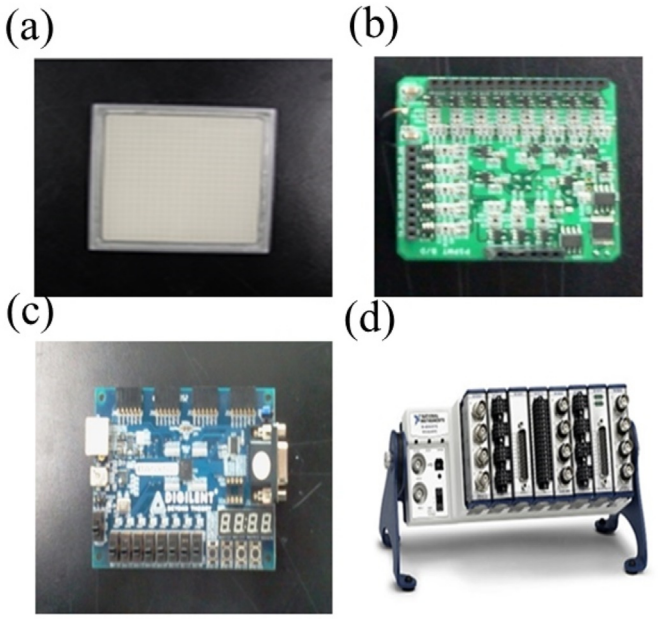

Fig. 2. Components of the imaging system: (a) CsI scintillator, (b) front-end circuit, (c) FPGA (SPARTAN3E), and (d) DAQ board (cDAQ-9178).

light non-uniformity of the multi-anode PSPMT's was corrected using a front-end circuit [20]. The extracted timing information from the front-end circuit was transmitted to the FPGA. The output of the FPGA triggered the DAQ board to send useful events to a computer. The distance between the center of the MURA coded mask and the radiation source was set to 30 cm, and the center of the CSI scintillator detector was positioned 3 cm apart from the center of the MURA coded mask. The activities of all point sources (511 keV (^{22}Na), 662 keV (^{137}Cs), 1173 keV and 1332 keV (^{60}Co)) for the experiment were 10 μCi. The measurement time was 1 h. The energy resolution of the pixelated CsI scintillator detector represented approximately 12% for 662 keV [21]. To obtain the reconstructed images using useful photoelectric events, appropriate energy windows around a photoelectric peak were applied. Table 1 shows the appropriate energy windows which was determined based on the measured energy resolution of a CsI scintillator detector at various energies.

As shown in Fig. 3, three separate collimation methods can be defined:

1. Only-mask method (case 1): the incident radiation passes through a MURA coded mask and forms shadow of mask on the detector. Consequently, all effective events form only-mask shadow image which is utilized for the image reconstruction.
2. Anti-mask method (case 2): after the only-mask is rotated by 90°, all holes of the original MURA coded mask pattern are replaced by opaque elements. The mask that becomes anti-symmetric by 90° rotation is known as the "anti-mask." The anti-mask method utilizes only the first shadow image using the background subtraction method for the image reconstruction.
3. Dual-anti mask method (case 3): the incident radiation passes through a mask and is measured first, and then the mask is rotated by 90° (anti-mask) and the incident radiation is measured again. Subsequently, the types of two different shadow images with the subtraction of background events can be acquired in the detector plane. The first shadow image can be obtained by subtracting shadow image of anti-mask from shadow image of only-mask, and the second shadow image can

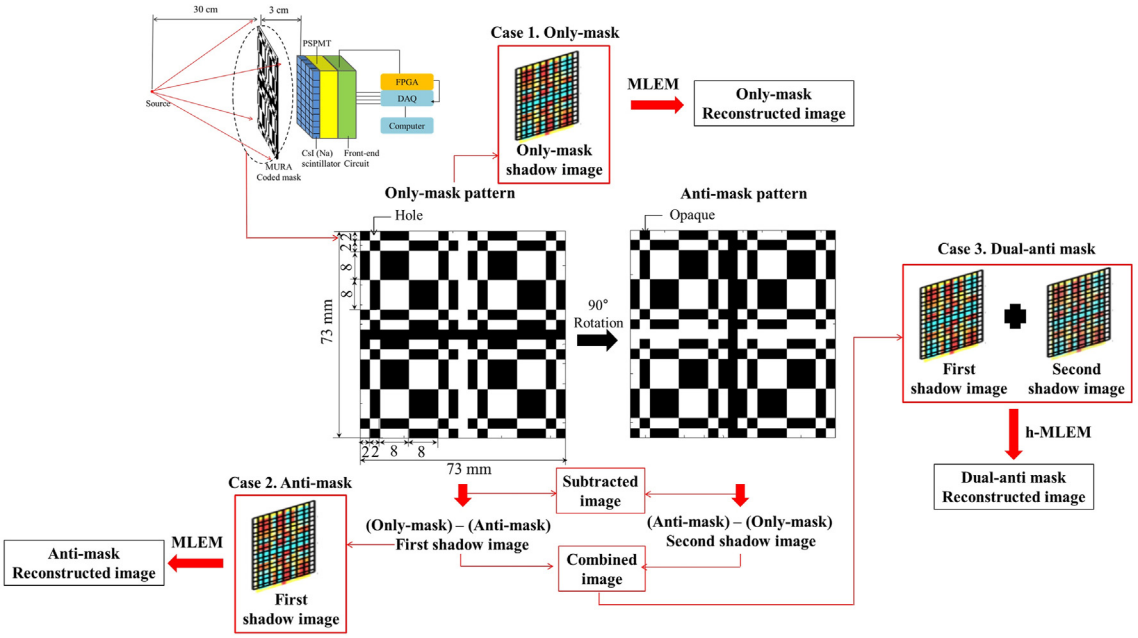

Fig. 3. Schematic diagram of the dual-anti mask imaging system with MURA coded aperture.

Table 1
Appropriate energy windows for photoelectric events at various radiation energies.

Energy (KeV)	Energy window for the photoelectric event (%)
511	476–546 keV (13.6%)
662	622–702 keV (12%)
1173	1120–1226 keV (9.0%)
1332	1275–1389 keV (8.5%)

be obtained in reverse order. Dual-anti mask method utilizes the information from both first shadow image and second shadow image simultaneously for the image reconstruction. We combined the datasets from the first shadow image and second shadow image using the h-MLEM [22].

The h-MLEM method was defined as shown in Eq. (1),

$$\lambda_j^{n+1} = \lambda_j^n \cdot \frac{\sum_i \frac{C_{ij}^F Y_i^F}{\sum_k C_{ik}^F \lambda_k^n} + \sum_i \frac{C_{ij}^S Y_i^S}{\sum_k C_{ik}^S \lambda_k^n}}{\sum_i C_{ij}^F + \sum_i C_{ij}^S}, \quad (1)$$

after the $(n+1)^{\text{th}}$ and nth iteration, the estimated values of a source pixel j are the λ_j^{n+1} and λ_j^n, respectively The superscripts F and S represent the first shadow image and second shadow image, respectively. C_{ij}^F and C_{ij}^S were elements of the system matrix for the dual-anti mask, which consisted of the attenuation in MURA coded mask. Y_i^F and Y_i^S were the two shadow images of the dual-anti mask after the subtraction of background events. The system matrix was calculated based on patterns of the MURA coded mask [11]. As the number of iterations increased, the reconstructed image using h-MLEM became sharper and noisier. Therefore, the resolution and noise (variance) were considered together to evaluate the reconstructed images. To quantitatively evaluate the reconstructed images, the resolution-variance curve (RV) and SNR were used.

For the coded aperture imaging system, the angular resolution which was represented by the full width half maximum (FWHM) of the point source image is defined simply by the distance (d) from the detector to the coded aperture and the width (c) of a MURA coded mask element [23].

$$\Delta\theta_{codedaperture} = 2tan^{-1}(c/2d). \quad (2)$$

The angular resolution was approximately 3.8° considering the focal length (3 cm) and mask pixel size. The results of the angular resolution were equivalent to the resolution limit which was between 3°–8° in the previous research. In order to obtain the relative standard deviation (RSTD), the raw data of each modality was divided into five subsets; the RSTDs were calculated based on the maximum pixel value in each subset. The SNR that represents the average value of the source pixel compared with the root mean square (RMS) of the background pixels in the reconstructed images at 20th iteration for each modality was calculated as [5,6].

$$Signal-noise-ratio(SNR) = \frac{\mu'_{signal}}{\sqrt{\frac{\sum(b_i - b')^2}{n}}}, \quad (3)$$

where, μ'_{signal} represents the average of the values in the source pixels, b_i represents the value of each pixel with the exclusion of the source pixels, and b' represents the average of b_i.

3. Results

Figurs 4-7 show the reconstructed images of each modality for various incident radiation energies. The pixel size of all reconstructed images was 2.2 × 2.2 cm^2. As the incident radiation energy increases, the performance of the blurred reconstructed images decreased because the penetration of the radiation through the MURA coded mask. Hence, the only-mask image of the point source is much more degraded than those of the background subtraction methods. However, using the shadow image that includes the subtraction of background events leads to a higher-performance reconstructed image. Especially, as the dual anti-mask method utilized two shadow images with reduced background noise, the performance of the dual-anti mask imaging was higher than that of

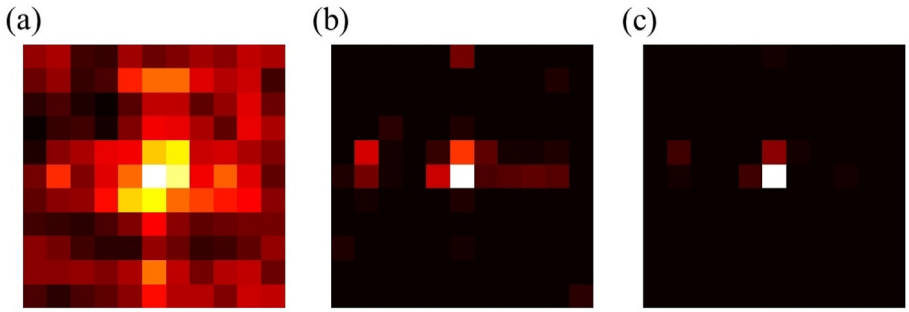

Fig. 4. Reconstructed image obtained using the MLEM and the h-MLEM method at 511 keV (20th iteration): (a) Only-mask, (b) anti-mask, and (c) dual-anti mask.

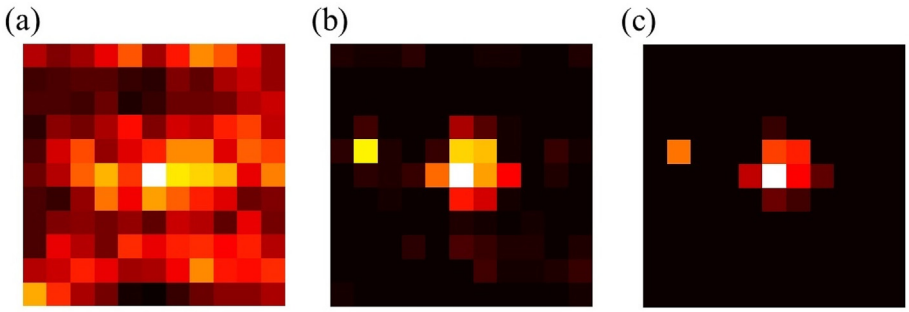

Fig. 5. Reconstructed image obtained using the MLEM and the h-MLEM method at 662 keV (20th iteration): (a) Only-mask, (b) anti-mask, and (c) dual-anti mask.

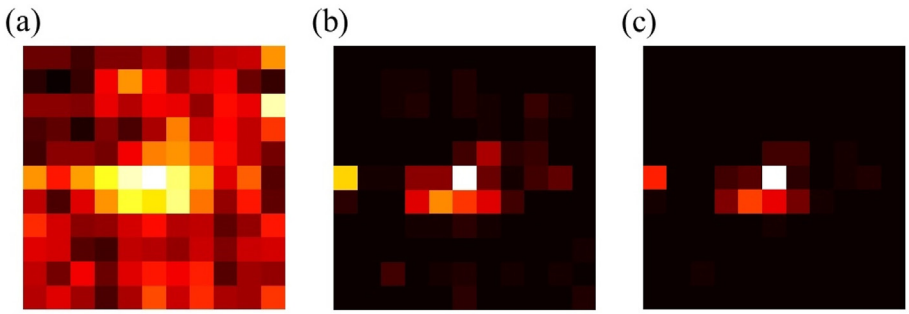

Fig. 6. Reconstructed image obtained using MLEM and the h-MLEM method at 1173 keV (20th iteration): (a) Only-mask, (b) anti-mask, and (c) dual-anti mask.

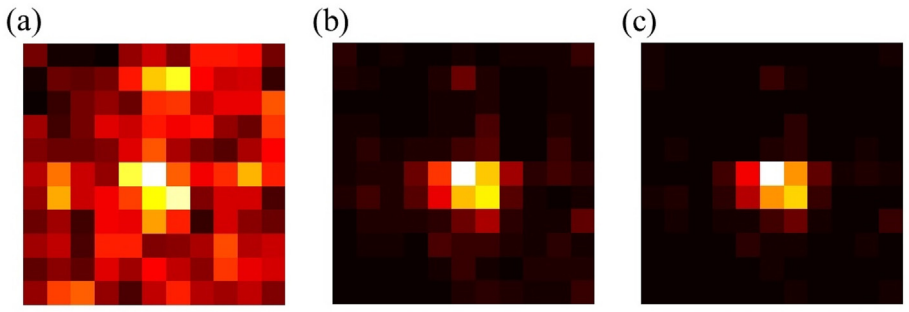

Fig. 7. Reconstructed image obtained using MLEM and the h-MLEM method at 1332 keV (20th iteration): (a) Only-mask, (b) anti-mask, and (c) dual-anti mask.

the conventional imaging. Further, by applying the h-MLEM method, all effective events of the dual-anti mask method could contribute to the reconstructed images. Hence, the reconstructed image obtained by the dual-anti mask method showed the high performance such as the least noise and the fewest artifacts among the three collimation methods.

Fig. 8 shows a quantitative evaluation of the reconstructed images using an RV curve. In RV curve, the data points are the values

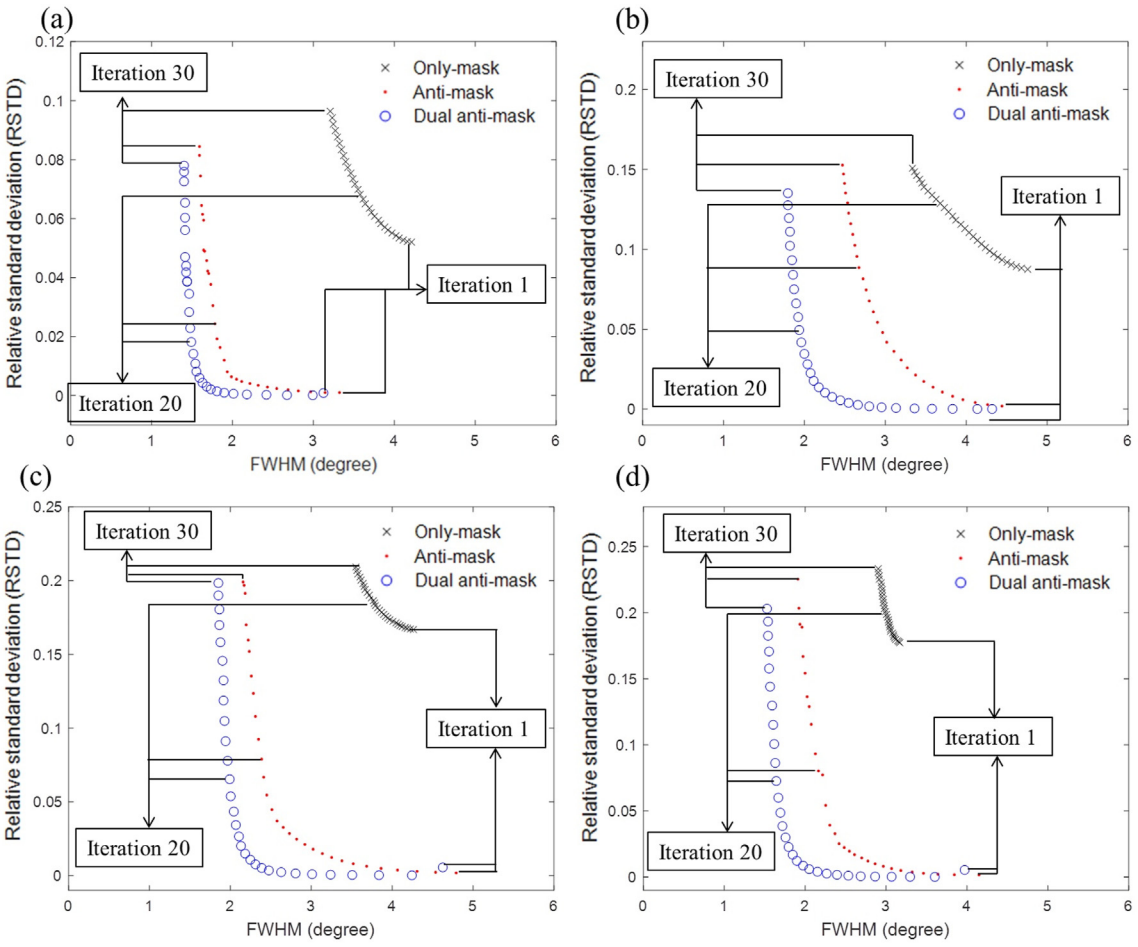

Fig. 8. Resolution-variance curve for a point source reconstructed by the h-MLEM method: (a) 511 keV, (b) 662 keV, (c) 1173 keV, and (d) 1332 keV.

for each iteration; the data points on the far-right sides are the values for the first iteration, and those of the far-left sides are the values for the final iteration. As the iteration number increases, the FWHM improves while the performance of RSTD decreases. Here, smaller values of RSTD and FWHM indicate better images hence a curve close to the origin indicates better performance. The RV curves of the dual-anti mask were closest to the origin in all radiation energies, because both shadow images contribute effectively to the reconstructed image. Hence, the RV curves prove that the performance of the dual-anti mask method is better than that of the conventional method.

Table 2 shows the performance comparison for each modality in reconstructed images. In all energies, the effective counts of only-mask method were higher than that obtained using the background subtraction methods. However, since the background was reduced in the shadow image of the subtraction methods, background subtraction methods presented higher performance than only-mask method. A 2.6 GHz CPU and MATLAB 2017b program were used for the image processing. The SNR of the reconstructed image based on each modality was calculated for various radiation energies and the iteration number was set to 20th iteration. At this iteration, the reconstructed images showed high resolution and without a significant noise peak. The SNR of dual-anti mask was highest among those of all collimation method. In summary, the

Table 2
Performance Comparison of each modality.

Energy (keV)	Collimation method	Effective counts	Computation time (sec)	SNR (20th iteration)
511	Only-mask	8412	7.7	5.2
	Anti-mask	2694	13.4	15.4
	Dual-anti mask	5534	30.1	22.0
662	Only-mask	7826	5.9	4.2
	Anti-mask	2107	10.6	13.4
	Dual-anti mask	5172	23.2	15.4
1173	Only-mask	5583	4.8	3.9
	Anti-mask	1791	9.8	8.2
	Dual-anti mask	3382	19.9	12.0
1332	Only-mask	4558	4.5	3.7
	Anti-mask	1516	9.4	7.7
	Dual-anti mask	2388	18.4	9.1

performance of the dual-anti mask method is superior to those of other methods due to the significant subtraction of the background.

4. Conclusions

The dual-anti mask method that integrates two different shadow images was developed, and its performance was evaluated and compared with that of the previously reconstruction methods. The reconstruction method of the h-MLEM was used to reconstruct each modality image. As two different shadow images can contribute effective information to the reconstructed images simultaneously, the results of the dual-anti mask method offer lower background noise in the reconstructed images. The RV curves and signal-to-noise ratios prove that the performance of the dual-anti mask method was better than that of the previously reconstruction methods. The results of this study demonstrated the availability of using dual-anti mask imaging as a means of monitoring the position and distribution of high energy nuclear materials.

Declaration of competing interest

The authors declare that they have no known competing financial interests or personal relationships that could have appeared to influence the work reported in this paper.

Acknowledgements

This work was supported by the Nuclear Safety Research Program through the Korea Foundation Of Nuclear Safety (KoFONS) using the financial resource granted by the Nuclear Safety and Security Commission (No. 1903006) and the National Research Foundation of Korea grant funded by the Korea government(MSIT) (No. 2020R1A2C1005924) of the Republic of Korea.

References

[1] E. Fenimore, Coded aperture imaging: predicted performance of uniformly redundant arrays, Appl. Optic. 17 (22) (1978) 3562–3570.
[2] E. Fenimore, T. Cannon, Coded aperture imaging with uniformly redundant arrays, Appl. Optic. 17 (3) (1978) 337–347.
[3] W. Cook, M. Finger, T. Prince, E. Stone, Gamma-ray imaging with a rotating hexagonal uniformly redundant array, IEEE Transactions on Nuclear Science NS- 31 (1998) 771–775.
[4] A. Goldwurm, K. Byard, A. Dean, C. Hall, J. Harding, Laboratory images with HURA coded apertures, Astron. Astrophys. 227 (1990) 640–648.
[5] P. Durrant, M. Dallimore, I. Jupp, D. Ramsden, The application of pinhole and coded aperture imaging in the nuclear environment, Nucl. Instrum. Methods Phys. Res. Sect. A Accel. Spectrom. Detect. Assoc. Equip. 422 (1999) 667–671.
[6] S. Gottesman, E. Fenimore, New family of binary arrays for coded aperture imaging, Appl. Optic. 28 (20) (1989) 4344–4352.
[7] T. Lee, W. Lee, Compact hybrid gamma camera with a coded aperture for investigation of nuclear materials, Nucl. Instrum. Methods Phys. Res. Sect. A Accel. Spectrom. Detect. Assoc. Equip. 767 (2014) 5–13.
[8] M. Cieślak, K. Gamage, R. Glover, Coded-aperture imaging systems: past, present and future development–A review, Radiat. Meas. 92 (2016) 59–71.
[9] Electric Power Research Institute, Use of Portable Gamma Detector Systems during Decommissioning, EPRI Report, 2019. TR-3002015953.
[10] S. Sun, Z. Zhang, L. Shuai, D. Li, Y. Wang, Y. Liu, X. Huang, H. Tang, T. Li, P. Chai, X. Jiang, B. Ma, M. Zhu, X. Wang, Y. Zhang, W. Zhou, F. Zeng, J. Guo, L. Sun, M. Yang, Y. Zhang, C. Wei, C. Ma, L. Wei, Development of a panorama coded-aperture gamma camera for radiation detection, Radiat. Meas. 77 (2015) 34–40.
[11] L. Smith, C. Chen, D. Wehe, Z. He, Hybrid collimation for industrial gamma-ray imaging: combining spatially coded and Compton aperture data, Nucl. Instrum. Methods Phys. Res. Sect. A Accel. Spectrom. Detect. Assoc. Equip. 462 (2001) 576–587.
[12] V. Paradiso, K. Amgarou, N. Lanaute, V. Schoepff, G. Amoyal, C. Mahe, O. Beltramello, E. Linard, A panoramic coded aperture gamma camera for radioactive hotspots localization, J. Instrum. 11 (2017) P11010.
[13] H. Kim, S. Ye, Y. Shin, G. Lee, G. Kim, Radiation imaging with a rotational modulation collimator (RMC) coupled to a Cs_2LiYCl_6:Ce (CLYC) detector, J. Kor. Phys. Soc. 69 (2016) 1644–1650.
[14] H. Kim, H. Choi, G. Lee, S. Ye, M. Smith, G. Kim, A Monte Carlo simulation study for the gamma-ray/neutron dual-particle imager using rotational modulation collimator (RMC), J. Radiol. Prot. 38 (1) (2018) 299–309.
[15] J. Braga, T. Villela, U. Jayanthi, F. D'Amico, J. Neri, A new mask-antimask coded-aperture telescope for hard X-ray astronomy, Exp. Astron. 2 (2) (1991) 101–113.
[16] R. Accorsi, F. Gasparini, R. Lanza, Optimal coded aperture patterns for improved SNR in nuclear medicine imaging, Nucl. Instrum. Methods Phys. Res. Sect. A Accel. Spectrom. Detect. Assoc. Equip. 474 (3) (2001) 273–284.
[17] T. Lee, S. Kwak, W. Lee, Investigation of nuclear material using a compact modified uniformly redundant array gamma camera, Nuclear Engineering and Technology 50 (6) (2018) 923–928.
[18] Online. Available: http://www.hamamatsu.com/jp/en/product/category/3100/3002/H8500C/index.html.
[19] Online. Available: http://www.hilger-crystals.co.uk/arrays.asp.
[20] V. Popov, S. Majewski, B. Welch, A novel readout concept for multianode photomultiplier tubes with pad matrix anode layout, Nucl. Instrum. Methods Phys. Res. Sect. A Accel. Spectrom. Detect. Assoc. Equip. 567 (2006) 319–322.
[21] W. Lee, T. Lee, 4π FOV compact Compton camera for nuclear material investigations, Nucl. Instrum. Methods Phys. Res. Sect. A Accel. Spectrom. Detect. Assoc. Equip. 652 (2011) 33–36.
[22] L. Schultz, M. Wallace, M. Galassi, A. Hoover, M. Mocko, D. Palmer, S. Tornga, R. Kippen, M. Hynes, M. Toolin, B. Harris, J. McElroy, D. Wakeford, R. Lanza, B. Horn, D. Wehe, Hybrid coded aperture and Compton imaging using an active mask, Nucl. Instrum. Methods Phys. Res. Sect. A Accel. Spectrom. Detect. Assoc. Equip. 608 (2) (2009) 267, 264.
[23] W. Lee, D. Wehe, M. Jeong, P. Barton, A dual modality gamma camera using $LaCl_3$(Ce) Scintillator, IEEE Trans. Nucl. Sci. 56 (1) (2009) 308–315.